Science Press

Cite this article as: Rare Metal Materials and Engineering, 2020, 49(10): 3402-3411.

ARTICLE

Strengthening Mechanism of Compositely Refined and Modified Multi-component Aluminum-silicon Alloy

Wang Zhengjun,   Zhang Man,   Zhang Qiuyang,   Lv Jianqiang

Huaiyin Institute of Technology, Huai'an 223003, China

Abstract: In order to improve the mechanical properties, a new Al-5Ti-1B-1RE master alloy refiner and Al-10Sr master alloy modifier were used to composite refine and modify the as-cast A356 aluminum alloy and a novel aluminum alloy composed of as-cast A356 aluminum alloy by adding Cu, Mn, Ti and other elements in a certain proportion. The morphology distribution of the second-phase particles and strengthening mechanism of the multi-component aluminum-silicon alloy were analyzed by OM, SEM, EDS, TEM and the electronic universal testing machine (CSS-44100). The results show that the second-phase eutectic silicon phase in the A356 aluminum alloy transforms from coarse lamellar to typical fibrous phase after the composite refinement and modification, and precipitates uniformly at the grain boundary of the soft-tough phase α-Al matrix. The grain size of the α-Al phase decreases significantly. It is mainly Hall-Petch grain boundary fine grain strengthening mechanism. In addition to the second-phase particle eutectic silicon in the novel aluminum alloy, there are other second-phase particles which are dispersed in the grain boundaries or intragranular. Various strengthening mechanisms work together. When the second-phase particles distribute on grain boundaries, it is mainly the Hall-Petch strengthening mechanism. When the second-phase particles distribute in intragranular, it is mainly Orowan strengthening mechanism, which becomes an effective obstacle to dislocation movement and plays a strengthening role.

Key words: compositely refining and modifying; second-phase particles; morphology distribution; Hall-Petch grain boundary fine grain strengthening; Orowan strengthening mechanism

---

Nowadays, the renewal speed of automotive core components such as engines is accelerating. The increasing emphasis on environmental protection, energy saving and emission reduction requires that the engine has a lighter weight but can adapt to more demanding environments and withstand higher fatigue resistance and wear resistance[1,2]. Aluminum and its alloys are the most ideal materials for meeting the lightweight requirements of today's automotive industry. They are known as "flying metals" and are widely used in automotive and other manufacturing industries due to their series of advantages[3-7]. The A356 aluminum alloy is one of the most widely used alloys in multi-element Al-Si alloys. It is a cast hypoeutectic Al-Si-Mg based aluminum alloy developed in the United States in the 1970s, due to its good

casting performance and comprehensive mechanical properties[8,9], which were introduced in the automotive industry shortly after the advent. With the rapid development of the automotive industry in the late 1980s, the A356 series of aluminum alloys have been more widely used in the automotive industry[10,11]. However, the mechanical properties, especially the plasticity, of as-cast A356 aluminum alloy without strengthening treatment are poor. The complex automotive parts put forward higher requirements for the mechanical properties and service properties of A356 aluminum alloy. Therefore, it is necessary to integrate more advanced processing technologies for A356 aluminum alloy in details. For example, under certain process specification conditions, composite refinement and modification and

---

alloying technologies can further improve the microstructure of the alloy and significantly enhance the mechanical properties of the alloy[12-14]. The mechanical properties of the cast A356 aluminum alloy mainly depend on the primary α-Al phase and the eutectic Si phase in its structure. At present, there are few reports on the simultaneous refinement and modification of A356 aluminum alloy [15]. Since the advent of Al-Ti-B master alloy refiner, it has become the most important and widely used grain refiner in the aluminum and aluminum alloy industry through continuous improvement, playing an incomparable advantage of other grain refiners[16-18]. However, due to its own performance defects, it is limited in the rolling of high-grade foils, and the refinement effect of the aluminum alloy (high-strength alloy) containing elements such as Zr and Cr is weakened or even lost, resulting in uneven grain structure, which is the so-called "refiner poisoning" phenomenon[19-21]. In recent years, through the continuous efforts of scientific research workers, the refinement, purification and degassing of rare earths have been combined with the refinement of Al-Ti-B master alloy[22]. A new type of green Al-5Ti-1B-1RE master alloy grain refiner has been developed. It has been found that rare earth can improve the morphology distribution of TiB_2 and $TiAl_3$ particles in Al-5Ti-1B and can refine the size of $TiAl_3$ particles, increase the number of heterogeneous crystal nuclei and improve the refinement effect[23]. It can solve the problem of TiB_2 aggregation, precipitation and refiner poisoning, and can improve or even eliminate the fatal defects existing in the Al-5Ti-1B master alloy grain refiner. At present, it is one of the most valuable and potential grain refiners for aluminum[24]. At the same time, a single Al-10Sr master alloy modifier is often used to modify the A356 aluminum alloy in industrial production to improve the morphology of eutectic Si and enhance its mechanical properties[25-27]. However, it has been proved[28] that after Sr modification treatment, due to the high activity of Al and Sr at high temperature, the oxidation is easy to worsen the surface density of the melt, and the surface is prone to obvious cracking, so that the fresh aluminum liquid is continuously exposed to the air, and the hydrogen content in the melt is greatly increased. Moreover, the refining effect of Sr modification alone on primary α-Al is limited. In view of the problems of coarse α-Al and easy to produce pores, how to overcome the shortcomings of single modifier Sr is still a hot spot in the research field of refinement and modification in aluminum-silicon alloys[29]. In recent years, it has been found that the introduction of rare earth into the new Al-5Ti-1B-1RE master alloy finer can form a dense oxide film on the surface of the melt, and almost no cracking phenomenon can be seen, thus significantly reducing the exposure probability of fresh liquid aluminum in the air. The hydrogen content in melt can be greatly reduced and the number of pinholes produced in castings can be reduced. The new Al-5Ti-1B-1RE master alloy finer has a strong refining effect on α-Al. Therefore, Al-5Ti-1B-1RE master alloy refiner and Al-10Sr master alloy modifier are selected to carry out composite refinement and modification treatment on A356 aluminum alloy, which can integrate refinement and modification treatment to achieve better results.

In addition to the composite refinement and modification of multi-component aluminum-silicon alloys, alloying has been one of the important means to improve mechanical properties and tap potential of materials. Some scholars can greatly improve the mechanical properties of the alloy by adjusting the content of Si, Mg, Cu, Mn, Ti and other elements in the aluminum-silicon alloy[30]. Therefore, alloying is still one of the important ways to obtain high strength and toughness cast aluminum alloy materials. However, as far as the strengthening mechanism of aluminum alloy is concerned, the research and analysis are mainly based on the premise that the second-phase particles are more evenly distributed in the alloy matrix, and the influence of the morphology distribution characteristics of the second-phase particles on the strengthening mechanism is mostly ignored, and there are few literature reports on the research in this respect[31]. The research work on the strengthening mechanism of materials has strong scientific significance and practical application value. But it is also very complicated and the focus of material science research in recent years, especially for multi-element aluminum alloy materials. This paper discussed a new Al-5Ti-1B-1RE master alloy refiner and Al-10Sr master alloy modifier was used to compositely refine and modify the as-cast multi- component A356 aluminum alloy and a novel aluminum alloy composed of as-cast A356 aluminum alloy by adding Cu, Mn, Ti and other elements in a certain proportion and the influence of the different morphology distribution characteristics of the second-phase particles on strengthening mechanism of the alloys, which have important guidance and application value for actual production, preparing high-quality new aluminum alloy and improving the aluminization rate of automobile manufacture.

1 Experiment

The experiment materials are mainly multi-component aluminum silicon A356 aluminum alloy (Si 7.02wt%, Mg 0.31wt%, Fe 0.08wt%, Al balance), Al-50Cu, Al-10Mn and Al-5Ti master alloys, Ti, KBF_4 powder, La-rich and Ce-rich mixed rare earth and industrial pure aluminum, Al-10Sr master alloy, special covering agent for aluminum and aluminum alloy, degassing agent, refining agent, coating, JJ-1 precision power electric stirrer and other auxiliary materials and tools are made by melt blending method. The burning loss rate of alloy elements shall be fully considered in the calculation of alloy element ingredients.

Firstly, Ti, KBF_4 powder, La-rich and Ce-rich mixed rare earth and industrial pure aluminum were weighed. Under certain technological conditions, Al-5Ti-1B-1RE master alloy

was prepared in KSL-12-JY well crucible resistance furnace by pure titanium particle method at 830 °C.

Secondly, graphite crucibles containing A356 aluminum alloys of equal mass were separately placed in three KSL-12-JY well resistance furnaces with identical condition to be heated to 750 °C. When the alloys became soft and concave, special covering agents for aluminum and aluminum alloy were sprinkled on the surface of the alloys, and after the alloys were completely melted, degassing, refining, stirring (In the following experiments, all the stirring were carried out using a JJ-1 precision power electric stirrer) and slag removal were carried out. The melt in the first furnace was cooled to 730 °C, slag removal, and poured to wedge-shaped metal die (In the following experiments, all the alloy melts were poured into a wedge-shaped metal mold of the same holding temperature). The second furnace melt, mass fraction of 0.80% the self-made Al-5Ti-1B-1RE master alloy refiner and 0.30% the Al-10Sr master alloy modifier were previously pressed into the graphite bell jar and then sequentially added to the melt, followed by stirring for 1 min, holding for 5 min, degassing, refining, slag removal, cooling to 730 °C, slag removal, pouring. At the same time, the melt in the graphite crucible of the third furnace was heated to 780 °C and Al-10Mn master alloy, Al-50Cu master alloy and Al-5Ti master alloy with certain mass were added in sequence under certain technological conditions. When each master alloy was added, the melt was subjected to forcefully stirring, heat preservation, refining, degassing, refining, slag removal and standing, cooling to 730 °C and slag removal. The chemical compositions of the three alloys (alloy I, II, III) were detected by IRIS ER/S full spectrum direct reading inductively coupled plasma emission spectrometer, as shown in Table 1. After that, the same percentage of refiner and modifier as that of the second furnace was added to carry out refinement and modification treatment, pouring and cooling. The three groups of alloys were sawed laterally along the middle position in turn to prepare metallographic samples. And their microstructures were characterized by LEICA DM 2500M transmission optical microscope and Hitachi S-3400N scanning electron microscope.

Finally, the above experiments were repeated once more. The three groups of cast samples (for convenience of writing, the aluminum alloy numbers of the above 1~3 furnaces treated by different processes were marked as sample I, II and III, respectively) were processed into rectangular cross-sectional area samples according to GB/T 228.1-2010 standard, as shown in Fig.1, and the tensile mechanical properties were tested on CSS-44100 electronic universal testing machine at a tensile rate of 1.00 mm/min. The Brinell hardness of the samples was tested on HBE-3000A electronic Brinell hardness tester. The diameter of the indenter was 5 mm, the load was 2450 N, and the holding time was 30 s. The test data of each group were the average of three samples.

2 Results and Discussion

2.1 Morphological distribution of second-phase particles in multi-aluminum-silicon alloys treated by different processes

The self-made Al-5Ti-1B-1RE master alloy and Al-10Sr master alloy were analyzed by X-ray diffraction with D/Max-2500/pc X-ray diffractometer. MDI jade5.0 analysis software was used to analyze the phase of the diffraction patterns. The second-phase particles of Al-5Ti-1B-1RE master alloy are mainly composed of Al, Al_3Ti, TiB_2 and $Ti_2Al_{20}RE$ phases, as shown in Fig.2a. The second-phase particles of Al-10Sr master alloy are mainly composed of Al and Al_4Sr phases, as shown in Fig.2b.

The morphology, the distribution and the component of the second-phases of the self-made Al-5Ti-1B-1RE master alloy and Al-10Sr master alloy were further analyzed by scanning electron microscope and EDS spectrometer with Hitachi S-3400N, as shown in Fig.3. Among them, the surface with a whitish phase, as indicated by the arrow A in Fig.3a, was analyzed by EDS spectrum, as shown in Fig. 4a, containing Al, Ti, RE. The atomic ratio is Ti:Al:(La+Ce)≈2:20:1. And combined with the result of X-ray diffraction in Fig.2, they could be identified as $Ti_2Al_{20}RE$ phase, ie $Ti_2Al_{20}La$, $Ti_2Al_{20}Ce$ phase. $Ti_2Al_{20}RE$ is combined by Al, Al_3Ti and RE. The size is large; the gray phase is irregular and block-like, with a clear angular, as indicated by the arrow B in Fig.3a. According to the EDS spectrum analysis, as shown in Fig. 4b, it mainly contains two elements of Al and Ti, and its atomic ratio is Al:Ti≈3:1 and they could be confirmed as Al_3Ti phase. The Al_3Ti phases of smaller sizes react almost completely with the rare earth element and transform into $Ti_2Al_{20}RE$, while the Al_3Ti phases of larger sizes have a stronger adsorption effect on the rare earth, resulting in many $Ti_2Al_{20}RE$ atomic groups. The results show that the phase sizes of Al_3Ti and $Ti_2Al_{20}RE$ are slightly larger. The small-sized

Table 1 Chemical compositions of the three alloys with and without refining and modification (wt%)

Alloy	Si	Mg	Cu	Mn	Ti	Fe	Else	Al
I	7.02	0.31	-	-	-	0.8	≤0.20	Bal.
II	7.02	0.31	-	-	-	0.8	≤0.20	Bal.
III	6.92	0.28	1.85	0.33	0.26	0.14	≤0.20	Bal.

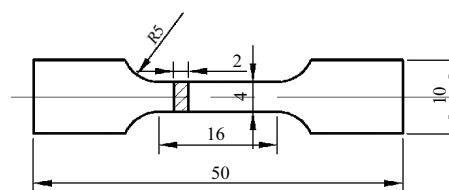
Fig.1 Size of sheet tensile specimen

Fig.2   XRD patterns of Al-5Ti-1B-1RE master alloy (a) and Al-10Sr master alloy (b)

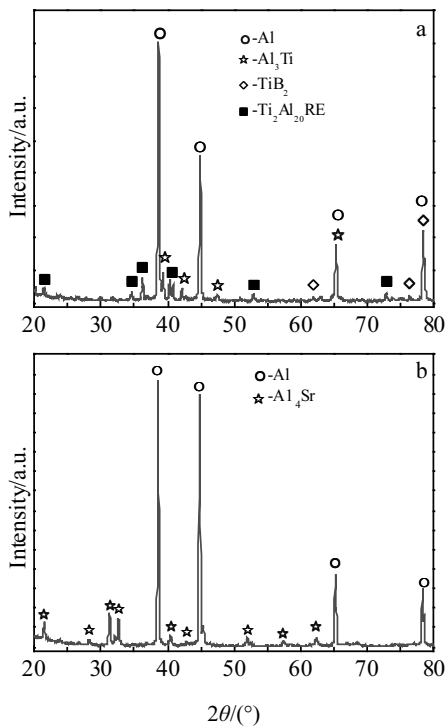Fig.3   SEM micrographs of Al-5Ti-1B-1RE master alloy (a) and Al-10Sr master alloy (b)

black-gray particles are mainly distributed around the Al_3Ti and $Ti_2Al_{20}RE$ phases or at the grain boundaries, as indicated by the arrow C in Fig.3a. According to the EDS spectrum analysis, as shown in Fig. 4c, the Ti and B elements, which have an atomic ratio of Ti:B≈1:2 could be determined to be TiB_2. The particle sizes are less than 1μm and the melting point is up to 2980 °C. They have very good chemical stability and do not react with RE.

The second-phase particles of Al-10Sr master alloy were analyzed, as shown in Fig.3b, in which the gray coarse plate-like compound is indicated by the arrow D. The EDS spectrum analysis, as shown in Fig.4d, indicates that it mainly contains two elements of Al and Sr, and the atomic ratio is Al:Sr≈4:1, which could be confirmed as Al_4Sr phase. The gray fine strip cluster compound on the matrix is indicated by the arrow E in Fig.3b. The EDS spectrum analysis, shown in Fig.4e, mainly contains two elements of Al and Sr, and the atomic ratio is Al:Sr≈49:1, which could be determined as eutectic phase ($Al+Al_4Sr$).

The morphology distribution characteristics of the second-phase particles in the matrix of A356 aluminum alloy treated by different processes are obviously different. Fig.5 is the microstructures of aluminum alloy samples I~III by different processes. It can be seen in Fig.5a that the sample I without refinement and modification has a large difference in the morphology of the eutectic Si of the second-phase particles,
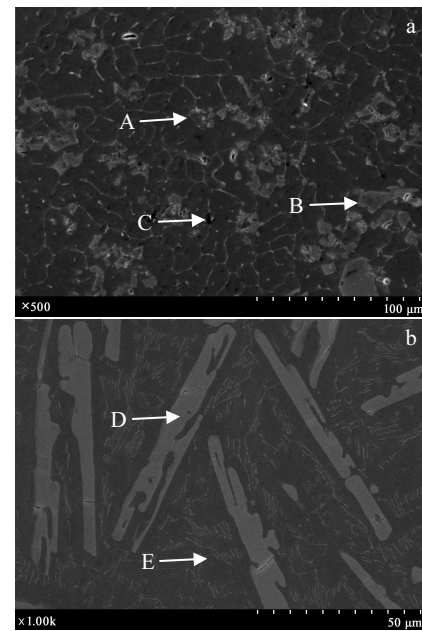
and presents coarse plate-like or long needle-like shape. The distribution in the aluminum matrix is non- directional and irregular, with sharp edges. Its size can be evaluated according to GB3246.1-2012 microstructure inspection method for aluminum and aluminum alloy processed products-linear intercept method. Most of them are 40~60 um, with a width of 4~6 um and the aspect ratio is more than 10, with obvious facet growth characteristics. The eutectic silicon with such morphology distribution is easy to generate stress concentration at the tip and edges, which significantly reduced the continuity of the matrix and splits the matrix. Fig.7 shows the mechanical properties of aluminum alloy samples I~III by different process. It can be seen that the tensile strength σ_b, yield strength σ_s, elongation δ and Brinell hardness *HB* of sample I are 177.56 MPa, 110.44 MPa, 1.17% and 687 MPa, respectively. Therefore, the mechanical properties, especially strength and plasticity are poor, but HB is still high.

As can be seen from Fig.5b, when the sample II is sub-jected to the refinement and modification of Al-5Ti-1B-1RE and Al-l0Sr master alloy, the shape and size of the matrix *α*-Al phase becomes more uniform and finer, the arrangement is tight, the shape is regular, and the grain boundaries are clearly visible. The secondary dendrites greatly reduce and are mainly fine and compact equiaxed crystal structures. The morphology of eutectic Si of second-phase particles changes significantly. The lamellar eutectic Si almost completely disappears and transforms into typical fibrous particles. The eutectic Si size is mostly between 1~2 μm, and its profile is clear, mainly distributed uniformly at grain boundaries. According to the
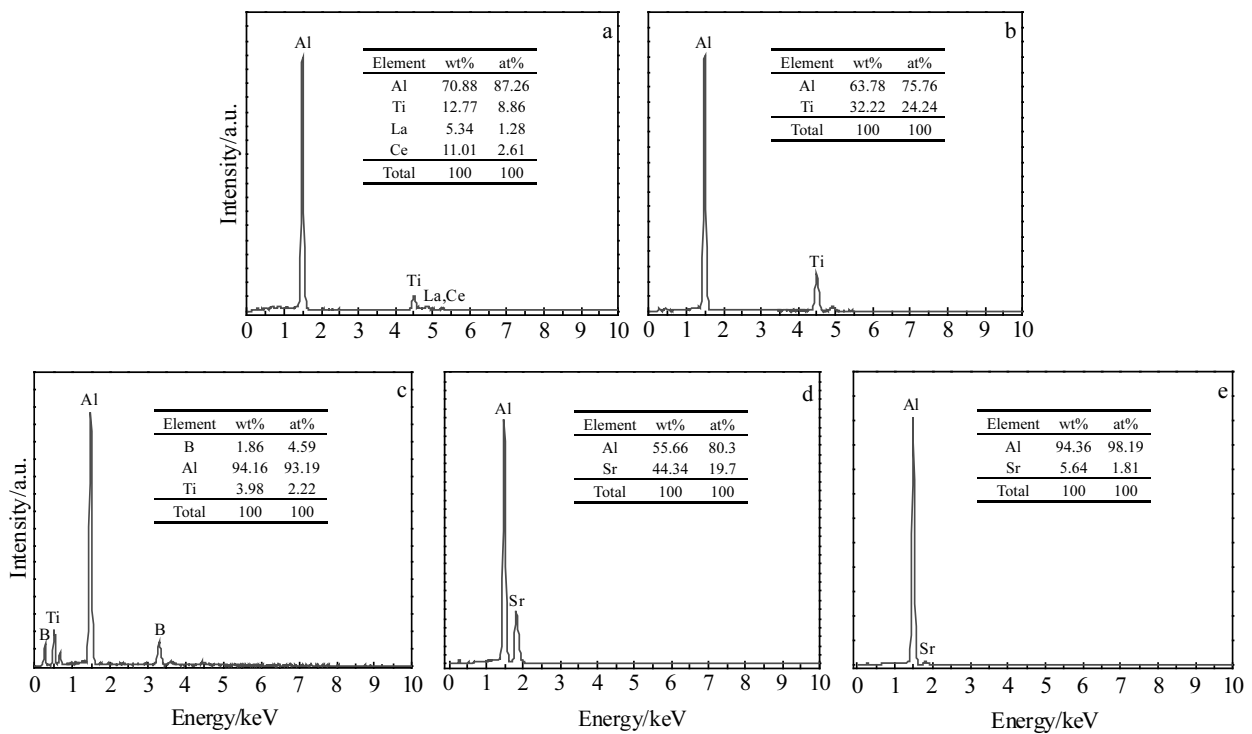
Fig.4   EDS spectra of the secondary phases of Al-5Ti-1B-1RE and Al-10Sr master alloy (points marked in Fig.3a and 3b): (a) point A, (b) point B, (c) point C, (d) point D, and (e) point E
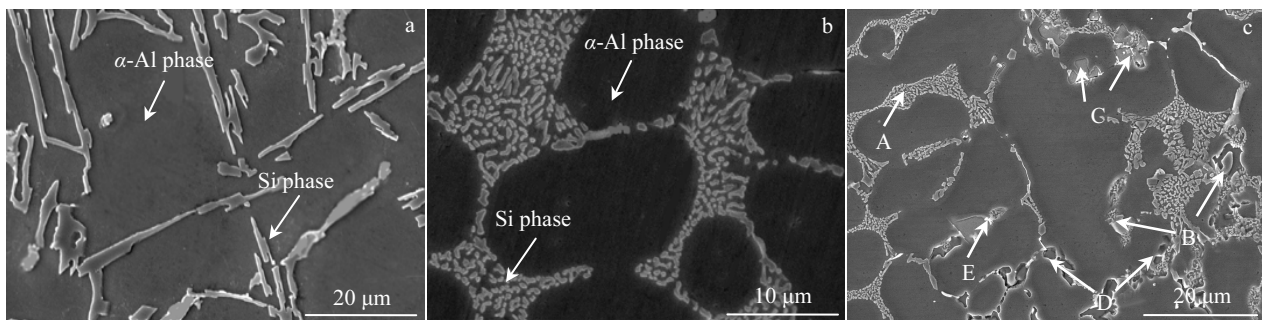

Fig.5   Microstructures of aluminum alloys by different process: (a) as-cast A356 alloy, (b) as-cast A356 alloy with 0.3% Al-l0Sr and 0.8% Al-5Ti-1B-1RE, and (c) the novel aluminum alloy with 0.3% Al-l0Sr and 0.8% Al-5Ti-1B-1RE

hypoeutectic Al-Si alloy modification grade chart provided by the American Foundry Association (AFS) as the evaluation standard [32], the eutectic Si is evaluated to be grade 5, which is completely modified. This is mainly due to the fact that when the Al-5Ti-1B-1RE master alloy refiner is added to the A356 aluminum alloy, the second-phase particles Al_3Ti, TiB_2 and $Ti_2Al_{20}RE$ mainly form, as shown in Fig.3a. Since TiB_2 and Al_3Ti in the melt have good wettability[33], the plane forms by the strong covalent bond B-B bond in the crystal structure. It is possible for Al_3Ti to nucleate on its surface, so Ti will preferentially form a Ti-rich layer around TiB_2 particles and

form an Al_3Ti cladding layer with Al, namely $Ti+3Al=Al_3Ti$. During the solidification process, a large amount of TiB_2 wrapped by a thin layer of Al_3Ti will serve as an effective nucleation substrate for α-Al, promoting nucleation and refining α-Al grains[34]. At the same time, the second-phase particle $Ti_2Al_{20}RE$ is dissolved to release the RE element. A protective thin layer forms on the surface of Al_3Ti, namely $Ti_2Al_{20}RE=14Al+2Al_3Ti+RE$. The block-shaped Al_3Ti is surrounded by an aluminum alloy rare earth phase, so that the Al_3Ti phase can exist longer in the aluminum melt, and the Al_3Ti formed on the TiB_2 particles is protected, further

Element	wt%	at%
Mg	0.38	0.55
Al	58.98	76.15
Si	1.32	1.64
Ti	0.18	0.13
Mn	0.44	0.28
Fe	0.51	0.32
Cu	38.19	20.94
Total	100	100

Element	wt%	at%
Mg	0.47	0.64
Al	61.57	75.98
Si	3.18	3.77
Ti	7.92	5.51
Mn	0.31	0.19
Cu	26.54	13.91
Total	100	100

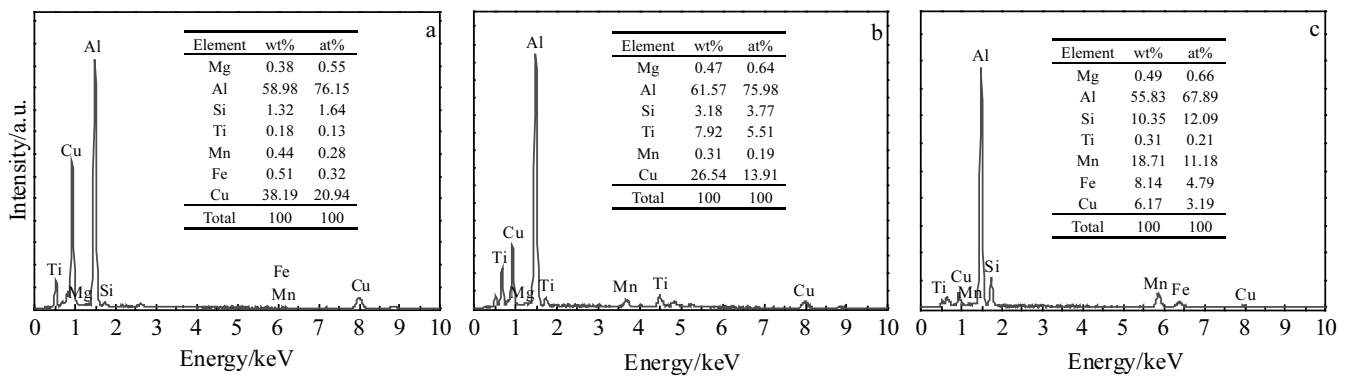| Element	wt%	at%
Mg	0.49	0.66
Al	55.83	67.89
Si	10.35	12.09
Ti	0.31	0.21
Mn	18.71	11.18
Fe	8.14	4.79
Cu	6.17	3.19
Total	100	100

Fig.6　EDS spectra of the novel aluminum alloy (points marked in Fig. 5c): (a) point B , (b) point C, and (c) point D

promoting the α-Al grain refinement. Since Al-l0Sr master alloy modifier is added to A356 aluminum alloy, the second-phase particle Al₄Sr forms, as shown in Fig.3b. However, only when Sr in the compound Al₄Sr is converted into a free Sr, i.e. the Al₄Sr=4Al+Sr transition occurs, and the refinement and modification can be exerted[5]. Free Sr is adsorbed and accumulated in the front of the growth interface of Si, which prevents eutectic Si from growing in flake form and produced twins. It makes eutectic Si branched much more frequently than unmodified eutectic Si, and makes the growth characteristics of eutectic Si change from anisotropy to isotropy. As a result, eutectic Si changes sharply from a mode of limited branching and coarse flake to a mode of fibrous growth with a large number of frequent branching[35]. Finally, the morphology and size of the eutectic Si have changed qualitatively. The stress concentration of eutectic silicon with such morphological distribution in the matrix is greatly reduced. The tensile strength σ_b, yield strength σ_s, elongation δ and Brinell hardness of the standard sample II are 242.06 MPa, 168.36 MPa, 7.54%, and 766 MPa, respectively, as shown in Fig.7. Compared with as-cast 356 aluminum alloy, its tensile strength σ_b, yield strength σ_s, elongation δ and Brinell hardness increase by 36.33%, 52.44%, 544.44% and 11.51%, respectively. The mechanical properties of the alloy are significantly improved, especially plasticity.

For sample III, as a novel aluminum alloy based on A356, it was alloyed with elements such as Cu, Mn and Ti and then subjected to composite refinement and modification, whose metallographic morphology is shown in Fig.5c. There are four main compounds: firstly, eutectic silicon phases，which distributed on the grain boundaries in the matrix have become fine fibers, and the sizes are mostly between 1~2 μm, as shown by the arrow A in Fig.5c. Secondly, the Cu-containing phases, generally, element Cu has a certain solubility in aluminum alloy, and the maximum solubility of Cu in aluminum is 5.65% at 548 °C. The solubility of Cu is 0.45% at 302 °C. The solubility of Cu in Al is reduced to less than 0.01% at room temperature, forming a limited solid solution with solid solution strengthening, but to a limited extent[36]. In the test, element Cu amounts to 1.85% in the alloy, and forms a supersaturated solid solution in Al. At the same time, some of the element Cu in the alloy cannot dissolve into the solid solution, which forms the second-phase, especially when combined with Mg, the strengthening effect is more significant, which can further improve the mechanical properties of the alloy at room temperature and high temperature. EDS analysis of the arrow B in Fig.5c is shown in Fig. 6a. It could be confirmed as Al₂Cu phases with small amount dissolved with trace elements Mg, Ti, Fe, and Mn and so on, which distributed in the crystals and the grain boundaries. The phases indicated by the arrow C in Fig.5c, according to the EDS spectrum analysis, are shown in Fig.6b. The phases containing AlCuMg, AlTi intermetallic compounds could be identified as AlSiTiCuMg. They are in the form of a small block, mainly distributed in the crystals and in the grain boundaries. Thirdly, the Mn-containing phases, as indicated by the arrow D in Fig. 5c, were analyzed by EDS as shown in Fig.6c. The phases with club-shaped or strip-shaped with rounded ends could be confirmed as AlSiCuFeMn, which are smaller in size than the AlSiTiCuMg phases and a small amount of Mg and Ti components are dissolved, which are mainly distributed in the crystals and in the grain boundaries. Finally, the RE- containing phases, the second-phase in which rare earth elements are dissolved, are mainly distributed on the grain boundaries and appear bright white, as indicated by the arrow E in Fig.5c. In a word, the microstructure of the novel aluminum alloy changes greatly with that of the refined and modified A356 aluminum alloy due to the appearance of the second-phase, which distributed uniformly and finely in the crystals and grain boundaries. In the process of tensile test, they become the main role of strengthening phases, which effectively improve the mechanical properties of the alloy. The tensile strength σ_b, yield strength σ_s, elongation δ and Brinell hardness are 282.36 MPa, 185.89 MPa, 6.96% and 968 MPa, respectively, by standard sample-III test, as shown in sample III of Fig.7.

Compared with the as-cast 356 aluminium alloy, its σ_b, σ_s, δ and HB increase by 59.02%, 68.32%, 494.87%, and 40.9%, respectively.

2.2 Analysis of strengthening mechanism

The mechanical properties of the material are closely related to its microstructure. The morphology distribution, size and bonding strength of the second-phase particles with the matrix determine the mechanical properties of the material, that is, the microstructure determines the properties. Eutectic Si granulation and spheroidization greatly reduces the splitting effect on the Al-Si alloy matrix, and can significantly improve the mechanical properties of the alloy, especially the plasticity. The microstructures of A356 aluminum alloy without refinement and modification are coarsened, and most of the dislocations slid out from the grains and entangle on grain boundaries in a large number. They intertwine and deliver each other, as shown in Fig.8a. Therefore, the stress concentration phenomenon at grain boundaries is serious. It is only necessary to add a small external force to induce dislocation motion in adjacent grains. That is to say, it is easy to cause the grain to slip, which makes the alloy deform and fracture easily, and the mechanical properties are low, as shown in sample I of Fig.7.

For sample-II, compactness and uniformity of the micro-structure of A356 aluminum alloy after refinement and modi-fication treatment are greatly improved. As the mechanical properties of A356 aluminum alloy mainly depend on the primary α-Al phase and eutectic Si phase. The α-Al phase is a solid solution of Si dissolved in Al (the maximum solid solubility of Si is about 0.05% at room temperature), similar to pure aluminum. The eutectic Si is equivalent to the second-phase in the alloy, which is hard and brittle and not easy to deform. Therefore, the morphology of Si phase has a particularly significant impact on the mechanical properties of A356 aluminum alloy. Since eutectic Si phase is mainly distributed at grain boundaries, according to grain boundary fine grain strengthening theory, Hall-Petch equation[37]:

Fig.7 Mechanical properties of aluminum alloys by different process

$$\sigma_s = \sigma_0 + kd^{1/2} \tag{1}$$

where, σ_s is yield strength, σ_0 is constant, roughly equivalent to the yield strength of a single crystal metal, d is the average size of the grain in polycrystal, and k is a constant showing the impact of grain boundary on the strength, which is related to the grain boundary structure, but little relevant with temperature.

It is known from Eq.(1) that the alloy strength σ_s increases as the grain size d decreases. This is mainly because the ratio of the surface area to the volume increases as the grain size d decreases, thereby increasing the surface tension. The surface tension causes the crystal lattice near the surface layer of the grain to be distorted, and the interaction force of the surrounding grains also causes the crystal lattice of the grain surface layer to be distorted. Due to the influence of these surface tension, a hard-to-deformation zone which hinders crystal deformation is generated near the grain boundary, and the alloy strength σ_s increases. At the same time, when the grain size is small, the number of dislocations entangled and intersected at grain boundaries is small, as shown in Fig.8b, and the degree of stress concentration is small. To activate dislocations in the adjacent grains, a large external force needs to be applied. The smaller the grain size, the larger the grain boundary area, the smaller the difference of strain angle between grain interior and near grain boundary, and the more uniform the deformation, the more difficult the corresponding deformation, and the larger force is required to make it slip, i.e. the greater the deformation resistance. The less the chance of cracking caused by stress concentration, the greater the stress and deformation before fracture, i.e. the higher the strength and elongation, the higher the mechanical properties, as shown in sample II of Fig.7.

For sample III, the second-phase particles Al_2Cu, AlTi, AlSiTiCu, AlSiCuFeMn and other phases are dispersed and precipitated evenly in the crystals and on the grain boundaries, which greatly improves the tensile strength and hardness of the alloy. Moreover, since the matrix is Al phase, the alloy is guaranteed to have certain plasticity, so the novel aluminum alloy, i.e. sample III has higher comprehensive mechanical properties. This is mainly due to the fact that when the second-phase particles are distributed on the grain boundaries, the theory of grain boundary fine grain strengthening is satisfied, i.e. the Hall-Petch formula is satisfied. The finer the grain, the higher the strength of the alloy. This is consistent with the test results of the mechanical properties of the aluminum alloys treated by different processes in Fig.7. For the rare earth phases accumulated at the grain boundaries, the diffusion of A1 element is hindered and the growth of crystal grains is hindered during the crystal growth of A1, which not only refines the α-Al crystal grains, but also modifies the needle-like eutectic Si. At the same time, the rare earth phases also play a role of pinning dislocations and further improve
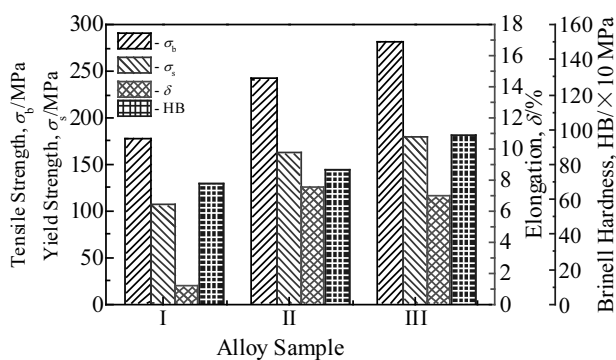
the mechanical properties. Moreover, due to the large difference between the thermal expansion coefficient of the second-phase particles and the matrix, the dislocation density inside the novel aluminum alloy is greatly improved, which also make the dislocation contribute greatly to the enhancement of the strength. When the second-phase particles are distributed in the crystals, it is known from Orowan's dislocation blocking theory that the hindrance to the dislocation motion is significantly enhanced and significantly larger than the distribution on the grain boundaries. According to the Orowan model[38], as shown in Fig.9, in which dislocations bypass the second-phases, when the dislocation line movement on Al matrix approaches the second-phase particles, they are obstructed and bent. With the increase of dislocation line bending, a dislocation half ring surrounding the second-phase particles is formed, and for remaining dislocation line returned to the straight line, dislocation lines move forward, which is also consistent with the test results in Fig.8c.

In this way, the resistance τ of dislocation movement can be expressed as[40]:

$$\tau = \frac{Gb}{2\lambda} \tag{2}$$

where G is the elastic modulus, b is the Berber's vector, and λ is the adjacent particle spacing.

It can be seen from Eq.(2) that by reducing the adjacent particle spacing λ, the radius of dislocation line passing through the second-phase particle becomes smaller, the curvature become larger, and the resistance τ for the dislocation motion become stronger. In the experiment, the size of eutectic silicon is basically below 5 μm, and other second-phase particles are also micron-sized. The particle phases are fine and numerous, which significantly increases the blocking effect of dislocation slip [41]. When dislocations bypass the particles, the dislocation loops are formed, and their curvature significantly increases, resulting in the increase of the alloy strength.

The adjacent particle spacing λ can be expressed by the following formula:

$$\lambda = d\left(\frac{\pi}{6V_f} - \frac{2}{3}\right)^{1/2} \tag{3}$$

where d is the average diameter of the particles, and V_f is the volume fraction of the second-phase particles.

According to the Orowan reinforcement formula[42]:

$$\sigma_{Orowan} = \frac{G_m b}{\pi(1-v)^{1/2}} \frac{1}{\lambda} \ln(d/b) \tag{4}$$

where G_m is the shear modulus of the matrix; b is the Poisson vector; v is the Poisson's ratio; λ is the particle spacing; and d is the average diameter of the second-phase particles.
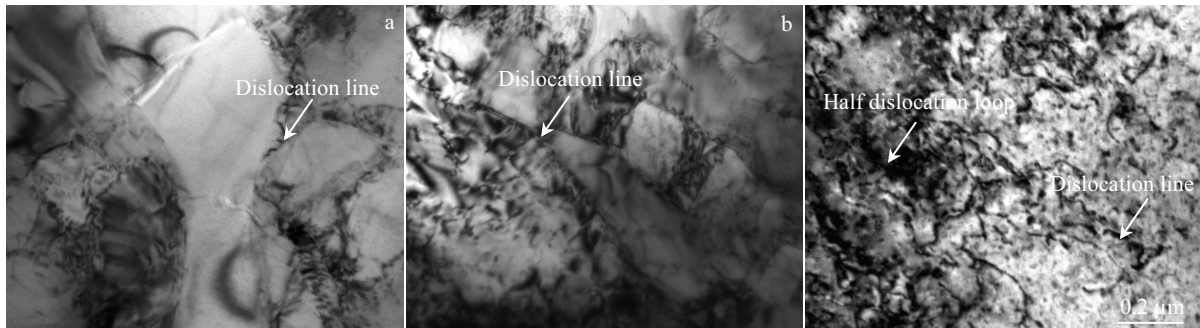
Substituting Eq.(3) into Eq.(4):

Fig.8　TEM images of dislocations in aluminum alloys treated by three different processes: (a) as-cast A356 alloy, (b) as-cast A356 alloy with refinement and modification, and (c) the novel aluminum alloy with refinement and modification

$$\sigma_{Orowan} = \frac{G_m b}{\pi(1-v)^{1/2}} \frac{1}{d\left(\frac{\pi}{6V_f} - \frac{2}{3}\right)^{1/2}} \ln(d/b) \tag{5}$$

It can be seen from Eq.(5) that to achieve a higher σ_{Orowan}, the average size d of the second-phase particles should be decreased or the volume fraction V_f should be increased. When the volume fraction of the second-phase particles V_f is constant, the smaller the diameter of the second-phase particles d, the more obvious the effect of Orowan strengthening. When the diameter of the second-phase particle d is constant, the
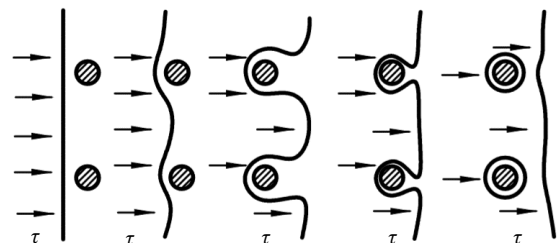

Fig.9　Schematic diagram of dislocations bypassing the second-phase particles[39]

effect of Orowan strengthening is enhanced as the volume fraction V_f of the second-phase particles increases. It can be seen that the smaller the diameter d of the second-phase particles, the larger the volume fraction V_f, and the larger the σ_{Orowan}, the more obvious the effect of strengthening. However, the smaller the diameter d of the second-phase particles, the larger the volume fraction V_f, the more difficult it is for the second-phase particles to disperse uniformly in the matrix.

Therefore, a large volume fraction V_f and small diameter d of second-phase particles uniformly dispersed in the matrix is the key to obtain a high-performance multi- component aluminum alloy material. Therefore, in the process of alloying and composite refinement and modification, JJ-1 precision power electric stirrer was used to stir strongly, which can make the grains collide with each other and move more strongly, so that the dendrite arms are sheared, broken and proliferated, especially between the liquid and the growing dendrites. This has contributed that the size of the second-phase particles decreases and the number increases after strong stirring. From Eq.(5), when the volume fraction V_f of the second-phase particles is constant, the smaller the diameter d of the second-phase particles, the better the effect of Orowan strengthening. So that the comprehensive mechanical properties of the novel aluminum alloy (the sample III) are significantly improved, as shown in sample III of Fig.7.

3　Conclusions

1) Among the multi-element Al-Si alloys treated by three different processes, the elongation δ of A356 Al alloy modified by self-made Al-5Ti-1B-1RE master alloy and Al-10Sr master alloy is the highest, reaching 7.54%. The strength and hardness of A356 Al alloy refined and modified by adding Cu, Mn, Ti and other elements are the highest. Compared with those of as-cast 356 aluminum alloy, its tensile strength σ_b, yield strength σ_s, elongation δ and Brinell hardness increase by 59.02%, 68.32%, 494.87% and 40.90%, respectively.

2) When the second-phase particles are distributed in the grain boundaries or crystals, various strengthening mechanisms work together. When they are distributed on the grain boundaries, it is mainly the grain boundary fine grain strengthening mechanism. When they are distributed in the crystals, it is mainly the Orowan strengthening mechanism.

References

1　Zhang Wenpei, Li Huanhuan, Hu Zhili *et al*. *Materials Review*[J], 2017, 31(7): 85

2　Li Yongbing, Ma Yunwu, Lou Ming *et al*. *Journal of Mechanical Engineering*[J], 2016, 52(24): 1 (in Chinese)

3　Ding Wanwu, Xia Tiandong, Zhao Wenjun *et al*. *Materials*[J], 2014, 7(2): 1188

4　Amie E B, Nami B, Shahmiri M *et al*. *Transactions of Nonferrous Metals Society of China*[J], 2013, 23 (9): 2518

5　Wang Zhengjun, Si Naichao, Wang Jun *et al*. *Journal of Materials Engineering*[J], 2017, 45(1): 20 (in Chinese)

6　Qiu Ke, Wang Richu, Peng Cahoqun *et al*. *Transactions of Nonferrous Metals Society of China*[J], 2015, 25(11): 3886

7　Zhang Jie, Zhang Dongqi, Wu Pengwei *et al*. *Rare Metal Materials and Engineering*[J], 2014, 43(1): 47

8　Zhou Jie, Bai Shan. *Aluminum Fabrication*[J], 2006, 32(3): 43 (in Chinese)

9　Lin Y. C, Luo Shuncun, Jiang Xingyou *et al*. *Transactions of Nonferrous Metals Society of China*[J], 2018, 28(4): 592

10　Wang Kui, Cui Chunxiang, Wang Qian *et al*. *Journal of Rare Earths*[J], 2013, 31(3): 313

11　Peng Jihua, Tang Xiaolong, He Jianting *et al*. *Transactions of Nonferrous Metals Society of China*[J], 2011, 21(9): 1950

12　Yu Jiliang, Li Zhongkui, Zheng Xin *et al*. *Rare Metal Materials and Engineering*[J], 2012, 41(11): 2054

13　Song Jiajia, Guo Deyan, Deng Chao *et al*. *Rare Metal Materials and Engineering*[J], 2013, 42(4): 756 (in Chinese)

14　Lei Ruoshan, Chen Guangrun, Wang Mingpu. *Rare Metal Materials and Engineering*[J], 2018, 47(9): 2607

15　Chen Xiang, Geng Huyuan, Li Yanxiang. *Acta Metallurgica Sinica*[J], 2006, 42(4): 1130 (in Chinese)

16　Yu Hong, Wang Ning, Guan Renguo *et al*. *Journal of Materials Science & Technology*[J], 2018, 34 (12): 2297

17　Kang Fuwei, Zhou Jie, Wang Zhiwei *et al*. *Rare Metals*[J], 2018, 37(8): 668

18　Xu Chao, Zhao Junwen, Luo Qinglai *et al*. *Rare Metal Materials and Engineering*[J], 2016, 45(6): 756

19　Yücel Birol. *Journal of Alloys and Compounds*[J], 2006, 22: 128

20　Ding Wanwu, Xu Chen, Hou Xingang *et al*. *Journal of Alloys and Compounds*[J], 2019, 776: 904

21　Vinod Kumar G S, Murty B S, Chakraborty M. *Journal of Alloys and Compounds*[J], 2005, 396(1-2): 143

22　Wang Zhengjun, Si Naichao. *Rare Metal Materials and Engineering*[J], 2015, 44(12): 2970

23　Chen Yajun, Xu Qingyan, Huang Tianyou. *Materials Review*[J], 2006, 20(12): 57

24　Wang Zhengjun, Si Naichao. *Rare Metal Materials and Engineering*[J], 2015, 44(6): 1494

25　Huang Zhixiang, Yan Hong, Wang Zhiwei. *Journal of Central South University*[J], 2018, 25(6): 1263

26　Lua L, Dahle A K. *Materials Science & Engineering A*[J], 2006, 435-436(5): 288

27　Chen Zhongwei, Ma Cuiying, Chen Pei. *Transactions of Nonferrous Metals Society of China*[J], 2012, 22(1): 42

28　Ouyang Zhiying, Mao Xiemin, Hong Mei. *Foundry*[J], 2006, 55(10): 1071 (in Chinese)

29　Dong Yun, Zheng Runguo, Lin Xiaoping *et al*. *Journal of Rare Earths*[J], 2013, 31(2): 204

30　Wang Jun, Si Naichao, Wang Zhengjun *et al*. *Materials Review B: Review Papers*[J], 2017, 31(2): 70 (in Chinese)

31　He Guangjin, Li Wenzhen. *Acta Materiae Compositae Sinica*[J], 2013, 30(2): 105 (in Chinese)

32　Chen Xiang, Geng huiyuan, Li Yanxiang. *Acta Metallurgica*

Sinica[J], 2005, 41(8): 891 (in Chinese)

33 Chen Yajun, Xu Qingyan, Huang Tianyou. *Journal of Tsinghua University, Science and Technology*[J], 2007, 47 (5): 618

34 Wang Zhengjun, Si Naichao, Wang Hongjian *et al*. *Rare Metal Materials and Engineering*[J], 2017, 46(1): 164 (in Chinese)

35 Zu Fangqiu. *Foundry*[J], 2011, 60(11): 1073 (in Chinese)

36 Cui Zhongqi, Tan Yaochun. *Metallography and Heat Treatment* [M]. Beijing: China Machine Press, 2007: 175 (in Chinese)

37 Lu Wenhua, Li Longsheng, Huang Liangyu. *Casting Alloy and Its Melting*[M]. Beijing: China Machine Press, 2012: 279 (in Chinese)

38 Yu Huashun. *Metal Matrix Composite Material and Preparation Technology*[M]. Beijing: Chemical Industry Press, 2006: 32 (in Chinese)

39 Wang Zhangzhong. *Fundamentals of Materials Science*[M]. Beijing: China Machine Press, 2018: 260 (in Chinese)

40 Banco D J, Kocks U F, Scattergood R O. *Philosophical Magazine* [J], 1973, 28 (6): 1241

41 Lee I S，Hsu C J, Chen N J *et al*. *Composites Science and Technology*[J], 2011, 71: 693

42 Aikin R M, Christodoulou L. *Scripta Metallurgica et Materialia* [J], 1991, 25(1): 9

复合细化变质多元铝硅合金的强化机制

王正军，张　满，张秋阳，吕建强

(淮阴工学院，江苏 淮安 223003)

摘　要：为改善力学性能，采用新型 Al-5Ti-1B-1RE 中间合金细化剂和 Al-10Sr 中间合金变质剂对铸态多元铝硅 A356 铝合金及在铸态 A356 铝合金中按一定比例添加 Cu、Mn、Ti 等元素组成的新型铝合金进行复合细化变质处理。采用光学显微镜（OM）、扫描电镜（SEM）及能谱（EDS）、透射电镜（TEM）和电子式万能试验机（CSS-44100）等技术对多元铝硅合金中的第二相粒子的形态分布特征及强化机制进行分析。结果表明：经复合细化变质处理的 A356 铝合金中的第二相粒子共晶硅相由粗大的片层状转变为典型的纤维状，在软韧相 α-Al 基体晶界处较均匀地析出，α-Al 相晶粒尺寸显著变小，其强化机制主要是第二相粒子共晶硅 Hall-Petch 晶界细晶强化；在新型铝合金中除第二相粒子共晶硅外，还存在其它弥散分布在晶界或晶内的第二相强化粒子，多种强化机制共同起作用。当强化粒子分布在晶界上时，主要是 Hall-Petch 强化机制；当分布在晶内时，主要是 Orowan 强化机制，成为阻碍位错运动的有效障碍，起到强化作用。

关键词：复合细化变质；第二相粒子；形态分布；Hall-Petch 晶界细晶强化机制；Orowan 强化机制

作者简介：王正军，男，1975 年生，博士，副教授，淮阴工学院机械与材料工程学院，江苏 淮安 223003，电话：0517-83559196，E-mail：wangzj2005@163.com